This is a repository copy of *Molten salt synthesis of Ce doped zirconolite for the immobilisation of pyroprocessing wastes and separated plutonium*.

White Rose Research Online URL for this paper:
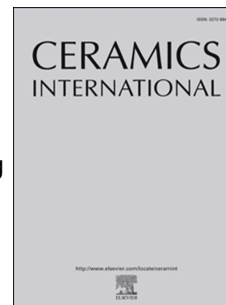https://eprints.whiterose.ac.uk/164861/

Version: Accepted Version

Journal Pre-proof

Molten salt synthesis of Ce doped zirconolite for the immobilisation of pyroprocessing wastes and separated plutonium

Amber R. Mason, Florent Y. Tocino, Martin C. Stennett, Neil C. Hyatt

Please cite this article as: A.R. Mason, F.Y. Tocino, M.C. Stennett, N.C. Hyatt, Molten salt synthesis of Ce doped zirconolite for the immobilisation of pyroprocessing wastes and separated plutonium, *Ceramics International* (2020), doi: https://doi.org/10.1016/j.ceramint.2020.08.080.

This is a PDF file of an article that has undergone enhancements after acceptance, such as the addition of a cover page and metadata, and formatting for readability, but it is not yet the definitive version of record. This version will undergo additional copyediting, typesetting and review before it is published in its final form, but we are providing this version to give early visibility of the article. Please note that, during the production process, errors may be discovered which could affect the content, and all legal disclaimers that apply to the journal pertain.

1 Molten salt synthesis of Ce doped zirconolite for the

2 immobilisation of pyroprocessing wastes and separated

3 plutonium

4 Amber R. Mason, Florent Y. Tocino, Martin C. Stennett, Neil C. Hyatt[*]

5 *Immobilisation Science Laboratory, Department of Materials Science and*

6 *Engineering, University of Sheffield, Sir Robert Hadfield Building, Sheffield S1*

7 *3JD, UK*

8 *[*]To whom correspondence should be addressed. Email*

9 *n.c.hyatt@sheffield.ac.uk, phone +44 (0) 114 222 5470, fax +44 (0) 114 222*

10 *5943*

11

12 ABSTRACT

13 Molten salt mediated synthesis of zirconolite $Ca_{0.9}Zr_{0.9}Ce_{0.2}Ti_2O_7$ was

14 investigated, as a target ceramic matrix for the clean-up of waste molten salts

15 from pyroprocessing of spent nuclear fuels and the immobilisation of separated

16 plutonium. A systematic study of reaction variables, including, reaction

17 temperature, time, atmosphere, reagents and composition, was made to

18 optimise the yield of the target zirconolite phase. Zirconolite 2M and 3T

19 polytypes were formed as the major phase (with minor perovskite) between

20 1000 – 1400 °C, in air, with the relative proportion of 2M polytype increasing

21 with temperature. Synthesis under 5% H_2/N_2 or Ar increased the proportion of

22 minor perovskite phase and reduced the yield of the zirconolite phase. The yield

23 of zirconolite polytypes was maximised with the addition of 10 wt.% TiO_2 and 5

24 wt.% TiO_2, yielding 91.7 ± 2.0 wt.% zirconolite, primarily as the 2M polytype,

25 after reaction at 1200 °C for 2 h, in air. The particle size and morphology of the

26 zirconolite product bears a close resemblance to that of the TiO_2 precursor,

27 demonstrating a dominant template growth mechanism. Although the molten

28 salt mediated synthesis of zirconolite is effective at lower reaction temperature

29 and time, compared to reactive sintering, this investigation has demonstrated

30 that the approach does not offer any clear advantage with over conventional

31 reactive sintering for the envisaged application.

32 **Keywords:** nuclear applications (E), spectroscopy (B), molten salt synthesis

33

34 **1. INTRODUCTION**

35 Pyrochemical reprocessing (pyroprocessing) is an advanced method of

36 recycling spent nuclear fuel (SNF) where the U, Pu and minor actinides (MA)

37 are separated from the fission products (FP) by electrorefining in a molten salt

38 eutectic [1]. An advantage of pyroprocessing over conventional aqueous

39 reprocessing is that a separated Pu stream is no longer generated, which

40 reduces the associated proliferation risk [2]. The waste stream generated via

41 this process is typically a chloride salt eutectic with entrained MA and FP, plus

42 trace residual Pu. Chloride rich waste streams such as these are challenging to

43 immobilise using traditional high level waste (HLW) immobilisation methods

44 since the chloride anion has low solubility in borosilicate glasses, which have,

45 hitherto, been applied for HLW immobilisation [3]–[7].

46 Zirconolite (prototypically $CaZr_xTi_{3-x}O_7$ where $0.8<x<1.35$) is a crystalline

47 titanate ceramic material and is the targeted actinide host phase in SYNROC C

48 [8]. It exists in the space group C2/c and has several polytypes: 2M, 3O, 3T, 4M

49 and 6T, with the most common being the monoclinic 2M structure [8–11]. In the

50 2M structure, Ca and Zr adopt 8- and 7-fold coordination, respectively, as CaO_8

51 and ZrO_7 polyhedra; whereas, Ti adopts mixed 6-fold and 5-fold coordination,

52 as TiO_6 and TiO_5 polyhedra, with the latter site being 50% occupied [12].

53 Synthetic zirconolite has natural analogue minerals retaining lanthanides and

54 actinides dated to be millions or hundreds of millions of years old, which further

55 demonstrates its long-term radiation stability and chemical durability over

56 geological timescales [13–16]. The lanthanide and actinide elements are usually

57 found on the Ca site with charge balancing cations, such as Al or Mg, on the Ti

58 site [8,16].

59 Molten salt synthesis (MSS) is a method of producing ceramic materials which

60 typically uses a chloride salt eutectic to reduce the diffusion distance of the

61 ceramic reagents. This method generally produces a material that is

62 homogeneous at a lower synthesis temperature and reaction time compared to

63 traditional solid state synthesis methods [17]. The chloride salts can be

64 dissolved upon completion of the reaction to recover the synthesised ceramic

65 material. Conventional solid state synthesis of zirconolite, requires reactive

66 sintering at 1450 °C for several hours, often with several cycles of heat

67 treatment and intermittent grinding [18]. In comparison, zirconolite can be

68 synthesised at 1200 °C in only a few hours, in the presence of a NaCl:KCl

69 molten salt eutectic, with a melting point of approximately 658 °C [19]. There

70 are two bounding mechanisms observed in the MSS of ceramic materials:

71 dissolution-precipitation and template growth [20–25], which are dependent on

72 the solubility of ceramic reagents in the salt eutectic. Dissolution-precipitation is

73 favoured when all reagents are comparably soluble in the salt eutectic and

74 subsequently react to form a product. Template growth occurs when one

75 reagent is less soluble and acts as a template onto which the other more

76 soluble reagents are deposited, at which point the product is formed. This

77 mechanism allows the microstructure of the sample to be controlled resulting in

78 uniform grain size and morphology.

79 This investigation seeks to develop the approach of decontaminating the

80 chloride molten salt waste from pyroprocessing, by using the salt itself as a

81 medium for the synthesis of a titanate ceramic wasteform to incorporate the

82 long lived lanthanides, MA and trace Pu [4,26–29]. Zirconolite was selected as

83 the titanate ceramic wasteform, with Ce utilised as a non-active structural

84 surrogate for the actinide and lanthanide elements due to having a similar ionic

85 radius, accessible oxidation states, and crystal chemistry [30–32]. The target

86 composition for the wasteform was $Ca_{0.9}Zr_{0.9}Ce_{0.2}Ti_2O_7$, where Ce was

87 substituted on both the Ca and Zr sites. This is a charge compensated

88 composition, targeting an equal proportion of Ce^{3+} ions on the Ca and Zr sites,

89 without the requirement of additional charge compensating species on the Ti

90 site. The target formulation was devised to incorporate Ce, as a MA / Pu

91 surrogate, at a realistic concentration for a conceptual ceramic wasteform.

92 The NaCl:KCl eutectic composition was chosen as a model system relevant to

93 wastes arising from pyrochemical reprocessing of mixed oxide $(U,Pu)O_2$ fuels

94 using the Dimitrovgrad Dry Process at the Research Institute for Atomic

95 Reactors in Russia and early pyrochemical reprocessing of short cooled

96 Experimental Reactor Breeder II metallic fuel at Argonne National Laboratory –

97 West (now Idaho National Laboratory), USA [33,34]. Additionally, a NaCl:KCl

98 eutectic was used in experimental pyrochemical reprocessing of thorium high

99 temperature reactor fuels undertaken at Joint Research Centre-Institute for

100 Trans Uranium Elements (JRC-ITU) [35]. The UK is also undertaking strategic

101 assessment of pyrochemical recycle of used nuclear fuels, including design and

102 demonstration of wasteforms for decontamination and immobilisation of

103 lanthanides and residual actinides from alkali chloride molten salts.

104 A further motivation for our research is management of the UK plutonium

105 stockpile, which is projected to exceed 140 tons at the end of current

106 reprocessing options [27]. A significant fraction of the plutonium stockpile will

107 require immobilisation in a suitable waste form, since it is unsuitable for reuse in

108 MOX fuel, which is the preferred management approach at the present time

109 [34]. Some of this material is contaminated by chlorine, as a result of the

110 degradation of the polyvinylchloride packaging used to store the material [28]. A

111 zirconolite ceramic is the leading candidate waste form for immobilisation of this

112 stockpile and, therefore, a rapid and low temperature MSS process could be

113 advantageous for ceramic waste form manufacture, given the presence of

114 chlorine as a contaminant. Gilbert previously established the NaCl:KCl eutectic

115 to be the most advantageous for zirconolite synthesis [19], although the yield

116 was only 86 wt.% after reaction at 1000 °C. In contrast, the yield of zirconolite

117 was 24 wt.% in the case of $CaCl_2$:NaCl eutectic at 1000 °C, whereas zirconolite

118 failed to form when utilising a $MgCl_2$:NaCl eutectic. Note that this work focused

119 the synthesis of the stoichiometric parent phase but did not consider the

120 incorporation of a MA/Pu surrogate. Our choice of NaCl:KCl eutectic

121 composition as the MSS medium was also made with due regard to potential

122 application to the immobilisation of chloride contaminated plutonium stockpile

123 material in a zirconolite ceramic, using Ce as a Pu surrogate.

124

2. MATERIALS AND METHODS

125

126   A NaCl:KCl eutectic (1:1 molar ratio) with a salt to ceramic molar ratio of 7:1

127   was primarily used in this study with the aim of producing single phase Ce

128   doped zirconolite. To optimise the yield of the target zirconolite phase, the

129   following reaction variables were systematically investigated: salt to ceramic

130   ratio (3:1 – 9:1), synthesis temperature (1100 °C – 1400 °C), time at synthesis

131   temperature (2 – 8 h), atmosphere (air, Ar or 5% H_2/N_2), Ce source (CeO_2 or

132    $CeCl_3.7H_2O$), stoichiometric or excess quantities of ZrO_2 and TiO_2 reagents

133   (excess, respectively, of 10 wt.% and 5 wt.%).

2.1.   Materials

135   CaO (Alfa Aesar purity 98%), TiO_2 (anatase) (Sigma Aldrich, 99% purity), ZrO_2

136   (Sigma Aldrich, purity 99%), $CeCl_3.7H_2O$ (Sigma Aldrich, >99% purity) and

137   CeO_2 (Fisher Scientific purity >99%) were used as reagents. NaCl (Sigma

138   Aldrich, purity 99%) and KCl (Sigma Aldrich, purity 99%) were used as the

139   molten salt flux. All reagents, with the exception of CaO and $CeCl_3.7H_2O$, were

140   dried overnight at 180 °C before use.

2.2.   MSS - $Ca_{0.9}Zr_{0.9}Ce_{0.2}Ti_2O_7$

142   A 1:1 molar ratio of NaCl and KCl was mixed (30 Hz, 5 mins) in a Fritsch

143   Pulverisette 6 planetary mill with cyclohexane as a carrier fluid to produce the

144   salt flux. Stoichiometric quantities of ceramic reagents were weighed according

145   to the composition $Ca_{0.9}Zr_{0.9}Ce_{0.2}Ti_2O_7$ and mixed using the same conditions as

146   the salt flux. A short mixing time was used to prevent size reduction of the

147   reagents and preserve the particle morphology, to assist later assessment of

7

148 the role of templating or dissolution-precipitation reaction mechanism. A 0.5 g

149 batch with a molar ratio of 7:1 salt eutectic:ceramic was mixed in a Fritsch Mini

150 Mill 23 with cyclohexane as a carrier fluid (30 Hz, 5 mins). The resulting slurry

151 was dried at ~95 °C, sieved through a 212 μm mesh to separate from the milling

152 media. The powder was uniaxially pressed in a 10 mm hardened stainless-steel

153 die with a 1 ton load and held for one minute to produce a green pellet. The

154 green pellets were placed in an alumina crucible and heated in a muffle furnace

155 to 300 °C for 1 h to remove any entrained moisture and then reacted at 1200 °C

156 for 2 h in air with a 5 °C/min heating/cooling rate. The resulting reacted pellet

157 was crushed into a fine powder using a pestle and mortar. The powder was

158 washed with deionised water to remove the salt flux and vacuum filtration used

159 to recover the product.

160 The above method was repeated with independent changes of experimental

161 variables as follows: salt to ceramic ratio (3:1, 5:1 and 9:1), synthesis

162 temperature (1100 °C, 1300 °C and 1400 °C), furnace atmosphere (flowing 5%

163 H_2/N_2 and Ar), furnace dwell duration (4 h and 8 h) and varying excess of ZrO_2

164 and TiO_2 reagents. Additionally, materials were produced using $CeCl_3.7H_2O$

165 (Sigma Aldrich, >99% purity), as the MA / Pu surrogate, replacing CeO_2 in the

166 ceramic batch.

167 After refinement of the experimental parameters discussed above, the optimum

168 synthesis conditions were used to produce Ce doped zirconolite using MSS,

169 with the resulting powder being uniaxially pressed into a ceramic body. The

170 ceramic body was placed into a furnace and reacted in air at 1350 °C for 20 h,

171 and the resulting ceramic was characterised.

8

172

2.3. Materials characterisation

174 Powder X-ray diffraction of reagents and products was performed with a Bruker

175 D2 Phaser X-ray Diffractometer with a Ni filtered Cu Kα radiation (λ = 1.5418 Å)

176 source, operating at 30 kV and 10 mA. Diffraction patterns were collected from

177 10° < 2θ < 70° with a step size of 0.02° 2θ and dwell time of 38 s per step. The

178 ICDD PDF-4+ database and ICSD sources were used to identify the phases

179 present in each sample. The PDF numbers used for the pattern identification

180 are: $CaZrTi_2O_7$ 2M (01-084-0163), $CaZrTi_2O_7$ 3T (01-072-7510), ZrO_2 (01-072-

181 1669), TiO_2 (16-934), CeO_2 (01-081-0792) and $CaTiO_3$ (01-082-0228). XRD

182 patterns were refined to provide quantitative phase analysis using the Bruker

183 TOPAS software [36].

184 Secondary electron imaging of the microstructure of reagents and ceramic

185 products was performed using a Philips XL 30 scanning electron microscope

186 (SEM) at a working voltage of 20 kV. The powders were mixed with isopropanol

187 in a beaker and placed in an ultrasonic bath. The resulting mixture was

188 mounted onto aluminium pin stubs using carbon tabs, allowing for the

189 isopropanol to evaporate before carbon coating.

190 The microstructure of the final sintered ceramic body was observed using a

191 Hitachi TM3030 SEM with Oxford Instruments Swift ED3000 silicon drift

192 detector. Energy dispersive X-ray spectroscopy (EDX) mapping was processed

193 using the Bruker Quantax 70 software with maps collected for a minimum of 10

194 minutes. The ceramic body was mounted in epoxy resin, polished to a 1 μm

195 optical finish and carbon coated prior to analysis.

196 The Ce oxidation state in each sample was determined from analysis of X-ray

197 absorption spectroscopy data at the Ce L_3 edge (5723.0 eV). Measurements

198 were conducted at the National Synchrotron Light Source II (NSLS-II) at

199 Brookhaven National Laboratory (Upton, New York) on beamline 6-BM. NSLS-II

200 operates at 3 GeV storage ring with a 400 mA current and 6-BM utilises a 3-

201 pole wiggler to deliver X-rays in the energy range between 4.5 and 23 keV. The

202 optical arrangement consists of a parabolic collimating mirror, a Si(111)

203 monochromator, a toroidal focussing mirror, and a harmonic rejection mirror.

204 For this study an unfocussed beam was used, and the beam size was limited to

205 0.5 mm in the vertical and 6 mm in the horizontal using slits. An ionisation

206 chamber was used to measure the incident X-ray energy and the fluorescence

207 signal was collected using a SII Vortex ME4 (4-element) Si drift detector. To

208 optimise collection efficiency, the samples were mounted at 45° to both the

209 incident X-ray beam and the vortex detector. The fluorescence signal was dead-

210 time corrected as previously described in Woicik et al. [37]. Spectra were

211 recorded between 5533 and 5965 eV with energy steps of 10 eV (5533 – 5693),

212 2 eV (5693 – 5713), 0.3 eV (5713 – 5783) and 0.05k (5783 – 5965). An

213 accumulation time of 0.5 s step^{-1} was used for the first three regions and 0.25k

214 step^{-1} for the final region. Multiple scans were collected for each sample and

215 averaged to improve the signal to noise ratio. To ensure energy reproducibility

216 (± 0.05 eV) a CeO_2 standard was measured simultaneously with each sample;

217 the CeO_2 standard was placed downstream of the sample and the transmitted

10

218   intensity was measured using an ionisation chamber. Absolute energy

219   calibration was performed by measuring a Cr foil and setting the position of the

220   first inflection point in the derivative spectrum to 5989 eV [38]. Samples, and

221   reference compounds, were prepared by homogenising finely powdered sample

222   with polyethylene glycol and uniaxial pressing to form a 13 mm pellet with a

223   thickness equivalent to 1 absorption length. Data reduction and linear

224   combination fitting (LCF) were performed using the Athena software package

225   [39] allowing the proportion of Ce^{3+} in each sample to be calculated.

226

3. RESULTS

We first attempted MSS of $Ca_{0.9}Zr_{0.9}Ce_{0.2}Ti_2O_7$ at 1200 °C with a 2 h reaction
time, in air, and a salt to ceramic ratio of 7:1 on a molar basis (the synthesis
conditions used by Gilbert to produce the parent $CaZrTi_2O_7$ zirconolite by MSS
[19]). However, secondary phases of ZrO_2 and $CaTiO_3$ were observed (Figure
1). Based on these results, several experimental parameters were varied to
achieve a single phase ceramic product (e.g. salt to ceramic ratio, temperature,
dwell duration, atmosphere, Ce source, excess reagents). It is desirable that a
single phase wasteform is obtained since the accessory perovskite phase may
also act as a host for Ce/Pu but has comparatively poor aqueous durability and
radiation tolerance [37]. We first investigated the effect of salt to ceramic ratio
(3:1, 5:1, 7:1, 9:1) on the MSS of $Ca_{0.9}Zr_{0.9}Ce_{0.2}Ti_2O_7$ at 1200 °C, with a 2 h
reaction time, in air. As shown in Figure S1, the phase assemblage was
observed to be invariant comprising a major zirconolite 2M phase, minor
perovskite, and trace zirconolite 3T, residual ZrO_2 and TiO_2 reagents.
Accordingly, the salt to ceramic ratio was fixed at 7:1, on a molar basis, in the
middle of the range investigated for further optimisation studies.

3.1 Characterisation of phase assemblage by X-ray diffraction

Figure 1 shows powder XRD patterns of the product recovered from MSS of
nominal $Ca_{0.9}Zr_{0.9}Ce_{0.2}Ti_2O_7$ over the range 1100 to 1400 °C, with a reaction
time of 2 h in air. All XRD patterns show the formation of zirconolite 2M and 3T
polytypes, at all temperatures, together with evidence of residual ZrO_2 and TiO_2
reagents, and an accessory perovskite phase (prototypically $CaTiO_3$).

250   Quantitative phase analysis of the phase assemblage was undertaken, by

251   Rietveld analysis of XRD data; the results are summarised in Table 1 and

252   compared in Figure 2 (an example fit is shown in Figure S2). The quantitative

253   phase analysis showed the overall yield of the zirconolite 2M phase to increase

254   with reaction temperature, from 43.9 wt.% at 1100 °C, to 62.1 wt.% at 1400 °C

255   (± 1.8 wt.%). A concomitant reduction in the fractions of residual ZrO_2 and TiO_2

256   reagents, accessory perovskite, and zirconolite 3T phase, were observed, with

257   increasing reaction temperature. The combined fraction of zirconolite 2M and

258   3T phases increased from 54.9 wt.% at 1100 °C, to 74.3 wt.% (± 2.0 wt.%) at

259   1400 °C. The reaction temperature was not increased further since single phase

260   Ce-doped zirconolites can be produced by conventional solid state synthesis at

261   1400 °C [19,20], and the MSS method of interest here would offer no

262   meaningful advantage.

263   Overall, these data show that at 1100 °C, the yield of zirconolite 2M was

264   hindered by slow reaction kinetics, at 1200 °C and higher temperature the yield

265   of zirconolite 2M was increased by reaction of reagents and conversion of the

266   zirconolite 3T to 2M polymorph. The overall yield of zirconolite phases

267   increased by a greater margin when the reaction temperature was increased

268   from 1100 °C to 1200 °C, compared to 1400 °C, which may reflect increased

269   volatilisation of the molten salt medium. For subsequent optimisation, a reaction

270   temperature of 1200 °C was selected, given the evidence for reasonable

271   reaction kinetics balanced against minimising the reaction temperature to

272   reduce evaporation of the molten salt and, with a view to process

273   implementation, potential volatile fission products.

13

274   Following investigation of the phase assemblage produced by MSS as a

275   function of reaction temperature, the effect of oxygen partial pressure was

276   studied by imposing an atmosphere of 5% H_2/N_2 or Ar gas. Figure 3 compares

277   the powder XRD patterns of the product recovered from MSS of nominal

278    $Ca_{0.9}Zr_{0.9}Ce_{0.2}Ti_2O_7$ at 1200 °C, with a reaction time of 2 h in air, 5% H_2/N_2 and

279   Ar. These data and the quantitative phase analysis summarised in Table 1 and

280   Figure 2, show the reducing atmosphere to result in a markedly lower yield of

281   zirconolite 2M and 3T phases. The combined yield of zirconolite 2M and 3T was

282   46.6 wt.% and 34.8 wt.% for the 5% H_2/N_2 and Ar atmosphere respectively,

283   compared to 66.9 wt.% for air atmosphere (± 2.0 wt.%). Evident from the

284   quantitative phase analysis is a greater fraction of residual ZrO_2 (15.6 – 17.3 ±

285   0.4 wt.%), which suggests that the solubility of ZrO_2 in the molten salt medium

286   is strongly dependent on effective oxygen partial pressure, resulting in a lower

287   yield of zirconolite and increased yield of perovskite (33.3 - 40.9 ± 1.0 wt.%). Ce

288   L_3 XANES data demonstrated Ce to be completely reduced to Ce^{3+}, which is

289   expected to stabilise the perovskite accessory phase as discussed further in

290   Section 3.3, possibly assisted by the reduction of Ti^{4+} to Ti^{3+} within the sample.

291   Begg and Clarke reported that annealing $CaZrTi_2O_7$ under 3.5 % H_2/N_2

292   atmosphere results in reduction of Ti^{4+} to Ti^{3+} [21,22], and the formation of a Zr

293   rich zirconolite and perovskite. Our observations are consistent with this

294   mechanism. Given the evident lower stability of the zirconolite phase under

295   reducing conditions, further optimisation of the MSS reaction conditions applied

296   a temperature of 1200 °C and air atmosphere.

14

297   Figure 4 compares the powder XRD patterns of the product recovered from

298   MSS of nominal $Ca_{0.9}Zr_{0.9}Ce_{0.2}Ti_2O_7$ after reaction at 1200 °C, with a reaction

299   time of 2 h, 4 h or 8 h in air. These data show a broadly similar phase

300   assemblage, with quantitative phase analysis, summarised in Table 1 and

301   Figure 2, revealing relatively small changes in phase fraction, close to the

302   estimated margin of precision. In particular, the total yield of zirconolite phases

303   did not show a marked increase with reaction time, with changes being close to

304   the estimated precision of ± 2.0 wt.%. This observation is consistent with

305   evaporation of the molten salt medium with increased reaction time, and with

306   diffusion – reaction occurring primarily in the solid state, for which the reaction

307   kinetics to yield zirconolite are known to be low at 1200 °C [19,20]. The

308   quantitative phase analysis of the product from reaction at 1200 °C in air for 4 h

309   showed an anomalously high fraction of residual ZrO_2 reagent, 3.9 ± 0.4 wt.%,

310   the origin of which is unclear, but is consistent with a marginally lower yield of

311   the target zirconolite phase. For the purpose of further optimisation of the MSS

312   process, therefore, the reaction conditions were fixed at 1200 °C, for a duration

313   of 2 h, under air.

314   With processing conditions of 1200 °C for 2 h in air, optimised from the

315   investigations above, the addition of excess ZrO_2 and TiO_2 reagents was

316   explored, with the aim of consuming the perovskite accessory phase. Figure 5

317   shows the powder XRD data pattern of the product recovered from MSS of

318   nominal $Ca_{0.9}Zr_{0.9}Ce_{0.2}Ti_2O_7$ after reaction at 1200 °C, for 2 h, in air, with an

319   excess of 10 wt.% ZrO_2 and 5 wt.% TiO_2 reagents. Quantitative phase analysis,

320   Table 1 and Figure 2, showed that this adjustment of the reaction composition

321 was successful and reduced the fraction of perovskite accessory phase to 9.4 ±

322 1.0 wt.%, with the yield of zirconolite 2M increased to 64.3 ± 0.8 wt.%. The

323 overall yield of zirconolite 2M and 3T phases, combined, increased to 83.6 ± 2.0

324 wt.%, with ca. 5 wt.% of unreacted reagents.

325 The use of $CeCl_3$ as a reagent and actinide surrogate, was also explored since

326 MA and Pu will be incorporated as a chloride species with the molten salt in a

327 pyroprocessing waste stream, unless precipitated as an oxide by oxygen

328 sparging [41]. Figure 5 presents the powder XRD data pattern of the product

329 recovered from MSS of nominal $Ca_{0.9}Zr_{0.9}Ce_{0.2}Ti_2O_7$ after reaction at 1200 °C,

330 for 2 h, in air, using $CeCl_3.7H_2O$ as the Ce source, with and without an excess

331 of 10 wt.% ZrO_2 and 5wt.% TiO_2 reagents. The overall yield of zirconolite 2M

332 and 3T phases, combined, was, respectively, 68.9 wt.% and 62.8 wt.% (± 2.0

333 wt.%) for the formulations with and without an excess of 10 wt.% ZrO_2 and 5 wt.

334 % $TiO_2.$ The use of $CeCl_3.7H_2O$ evidently has a detrimental effect on the phase

335 assemblage, compared to the use of CeO_2, with a reduced yield of zirconolite.

336 This is correlated with the residual ZrO_2 phase fraction being approximately

337 three times greater in the products of reaction utilising $CeCl_3.7H_2O$ compared to

338 CeO_2, suggesting the lower yield may arise from lower ZrO_2 solubility.

339 The final step in this study involved sintering of the product of

340 $Ca_{0.9}Zr_{0.9}Ce_{0.2}Ti_2O_7$ MSS, produced at 1200 °C, for 2 h, in air with an excess of

341 10 wt.% ZrO_2 and 5 wt.% TiO_2, using CeO_2 as a Ce source. The sintering

342 conditions were 1350 °C for 20 h in air, and X-ray diffraction, Figure 6, coupled

343 with quantitative phase analysis, demonstrated the combined zirconolite 2M, 4M

344 and 3T polymorphs to comprise 91.7 ± 2.0 wt.% of the phase assemblage, with

345 the 2M polymorph (75.9 ± 1.8 wt.%) as the major component. A minor

346 perovskite accessory phase was determined (7.3 ± 1.0 wt.%) with the trace

347 CeO_2, ZrO_2 and TiO_2 (combined 1.0 ± 0.5 wt.%).

348

3.2. SEM/EDX characterisation

350 The scanning electron micrographs in Figure 7 show the morphology of each

351 reagent, along with that of the $Ca_{0.9}Zr_{0.9}Ce_{0.2}Ti_2O_7$ product of MSS at 1200 °C

352 for 2 h, in air (with CeO_2). Comparison of the particle morphology of the

353 reagents and the product material, shows that the primary particle size and

354 habit of the product is similar to that of the TiO_2 reagent (~ 1 μm) and clearly

355 differentiated from the that of the CeO_2 and ZrO_2 reagents, with much larger

356 and smaller particle size, respectively. This suggests that template growth is the

357 mechanism by which $Ca_{0.9}Zr_{0.9}Ce_{0.2}Ti_2O_7$ was produced. The faceted nature of

358 TiO_2 reagent (see Figure 7 (a)) was reflected in the habit of the

359 $Ca_{0.9}Zr_{0.9}Ce_{0.2}Ti_2O_7$ product (Figure 7 (d)). However, it was evident that some

360 growth in product particle size had occurred, relative to the TiO_2 reagent, which

361 provides evidence for a contribution of dissolution – precipitation and/or solid

362 state diffusion, to the overall synthesis mechanism.

363 The microstructure of the sintered $Ca_{0.9}Zr_{0.9}Ce_{0.2}Ti_2O_7$ ceramic is shown in

364 Figure 8. The material comprises a majority matrix (mid grey) of the zirconolite

365 2M polymorph, with inclusions of ZrO_2 (bright grey) and small isolated

366 perovskite grains (dark grey). The zirconolite 3T polymorph cannot be

367 differentiated from the 2M polymorph, presumably due to similar composition

368 and hence back scattered electron contrast, combined with its low abundance.

369 The average EDX determined composition of the combined zirconolite 2M and

370 3T phases, was $Ca_{0.95(3)}Zr_{0.88(3)}Ce_{0.17(2)}Ti_{2.01(2)}O_7$, in reasonable agreement with

371 the target stoichiometry. This implies an average Ce oxidation state of $Ce^{3.2+}$,

372 within the zirconolite phase.

373 The zirconolite 4M phase is apparent as a small variation to the matrix contrast,

374 which arises from a slightly higher Ce concentration as judged from EDX data.

375 The microstructure is relatively well sintered although isolated porosity is

376 apparent.

377

3.3. Ce L$_3$ XANES

Ce L$_3$ XANES data were acquired from product materials as a probe of the

average Ce oxidation state and are shown in Figure 9. The spectra were

analysed using linear combination fitting (LCF) to estimate the proportion of

Ce^{3+} in each product, using reference spectra of CeO$_2$ (for 8-fold coordinated

Ce^{4+}), CeAlO$_3$ (for 12-fold coordinated Ce^{3+}) and CePO$_4$ (monazite; for 9-fold

coordinated Ce^{3+}). Spectra were fitted over the range 5700 – 5760 eV, under

the constraint that the fractional weights of the reference spectra sum to unity;

the results are summarised in Table 2 with an example fit shown in Figure S3.

Note that the Ce L$_3$ XANES of CePO$_4$ and CeAlO$_3$ present a single intense

feature on the rising absorption edge, whereas CeO$_2$ presents three features, of

lower relative intensity, for which the corresponding final state electron

configurations were previously assigned [42–45].

The Ce L$_3$ XANES data and LCF analysis (Figure 9A; Table 2), showed the

fraction of Ce^{3+} to increase with increasing reaction temperature (with constant

reaction time of 2h, in air), which is expected for the autoreduction of CeO$_2$ [46];

this was correlated with the concomitant increase in the combined fraction of

major zirconolite 2M and 3T polytypes, and reduction in the perovskite fraction,

in the phase assemblage (Table 1). In contrast, the fraction of Ce^{3+} increased

only marginally when the reaction time was extended from 2h to 8h (Figure 9C;

Table 2), consistent with only a small increase in the combined fraction of major

zirconolite 2M and 3T polytypes, and reduction in perovskite phase fraction

(Table 1). Taken together, these data show that the total yield of zirconolite and

Ce^{3+} fraction increase with increasing temperature, according to the target

402 formulation, by reaction of the perovskite accessory phase and residual TiO_2

403 and ZrO_2. It is evident, however, that the zirconolite product must incorporate

404 some proportion of Ce^{4+}.

405 Synthesis in a reducing atmosphere showed a complete reduction of Ce with

406 the fraction of Ce^{3+} being $100 \pm 4\%$ for both 5% H_2/N_2 and Ar products (Figure

407 9B). This was accompanied by a significant decrease in zirconolite yield in

408 contrast with the effect of increasing temperature on phase assemblage. This

409 implies that when the Ce^{3+} content increases above ca. 60%, the competing

410 perovskite phase is stabilised, which provides a 12 co-ordinate site to

411 accommodate the larger Ce^{3+} species [49]. The proportion of perovskite phase

412 is similar to the ~ 40 wt.% observed in the phase assemblage produced from

413 conventional reaction sintering of $CaZr_{0.6}Ce_{0.2}Ti_2O_7$ ceramics under H_2/N_2 and

414 Ar, with a Ce^{3+} content of 80 – 100% [47].

415 Substituting $CeCl_3$ for CeO_2 as the Ce source, resulted in reduction of the Ce^{3+}

416 fraction from $59 \pm 3\%$ to $38 \pm 3\%$, in the products from reaction at 1200 °C for 2

417 h, in air; however, this was not accompanied by a significant change in the

418 overall phase assemblage. The effect of addition of 10 wt.% ZrO_2 and 5 wt.%

419 TiO_2 to the formulation resulted in marked reduction of the Ce^{3+} fraction from 59

420 $\pm 3\%$ to $33 \pm 3\%$, in the product from reaction at 1200 °C for 2h, in air,

421 correlated with the maximum yield in of combined zirconolite 2M and 3T

422 polytypes in the phase assemblage (Table 1); this is also the case when CeO_2

423 is replaced by $CeCl_3$, although to less extent. Taken together, these data

424 demonstrate a strong effect of the addition of excess 10 wt.% ZrO_2 and 5 wt.%

20

425   TiO_2 in increasing the total yield of the zirconolite product, which must

426   incorporate a higher fraction of Ce^{4+}.

427   Figure 10 shows a comparison between the average Ce oxidation state (from

428   Table 2) and the weight fraction of perovskite formed in each product. There is a

429   general trend of increasing perovskite content associated with a greater the

430   quantity of Ce^{3+} in the sample at a constant synthesis temperature. As noted

431   above, the competing perovskite phase provides a 12 co-ordinate site to

432   accommodate the larger Ce^{3+} species [40], and hence the proportion of the

433   perovskite phase increases with increasing Ce^{3+} content, which is generally

434   associated with a lower yield of zirconolite.

435

436   **4. DISCUSSION**

437   Ce doped zirconolite was synthesised in a NaCl:KCl molten salt eutectic, as a

438   conceptual process for decontamination of pyroprocessing molten salt wastes

439   and immobilisation of separated plutonium. The presence of a molten salt

440   eutectic enables synthesis of zirconolite at 1200 °C in 2 h, in air, considerably

441   reduced compared to conventional reaction sintering which requires e.g. 1400

442   °C for 20 h. Interestingly, our investigation yields zirconolite 2M, 3T and 4M

443   polytypes, with evidence for conversion of 3T to 2M, with increasing

444   temperature. In contrast, similar compositions fabricated by conventional

445   reactive sintering comprise only the 2M polytype, with minor 4M polytype when

446   synthesised under air [48]. Our data are consistent with previous studies of

447   NaCl:KCl and $CaCl_2$:NaCl molten salt synthesis of the parent $CaZrTi_2O_7$

448   zirconolite, which identified the formation of the 3T polytype, as the major phase

21

449 after reaction at 1100 °C, giving way to formation of the 2M polytype at 1200 °C

450 [19]. The zirconolite 3T phase therefore appears to be a low temperature

451 metastable polytype structure.

452 Molten salt mediated synthesis yields products with a minimum Ce^{3+} content at

453 least 33% greater than similar compositions synthesised by reactive sintering in

454 air, when using CeO_2 as a reagent. Therefore, the mechanism of Ce solubility in

455 the NaCl-KCl eutectic appears to involve reduction of Ce^{4+} to Ce^{3+}, yielding

456 products with relatively high Ce^{3+} content. We are not aware of solubility data

457 for Ce^{4+} / Ce^{3+} in chloride molten salts, but this conclusion is consistent with

458 chloride molten salt mediated synthesis of CeOCl from CeO_2 [48]. Interestingly,

459 the analogous $CaZr_{1-x}Pu_xTi_2O_7$ system is reported to yield the zirconolite 3T

460 polytype on reduction of Pu^{4+} to Pu^{3+} and zirconolite 3T natural analogues are

461 generally characterised by a high fraction of trivalent lanthanides [49,50].

462 Hence, whilst $CaZrTi_2O_7$ can evidently be stabilised in the 3T polytype up to

463 1100 °C, incorporation of a significant Ce^{3+} may assist in stabilising this

464 polytype to higher temperature as reported herein.

465 Perovskite is formed as an accessory phase in all products characterised in this

466 study, with increased perovskite fraction correlated with increased Ce^{3+} fraction

467 at constant synthesis temperature (1200 °C). As noted in the introduction, the

468 formation of perovskite is undesirable since it has been shown to incorporate

469 actinides but demonstrates comparably lower radiation tolerance and durability,

470 with respect to zirconolite [51]. Nevertheless, the perovskite phase fraction

471 could be reduced to 7.3 ± 1.0 wt.%, by adjusting the formulation to incorporate

472 10 wt.% ZrO_2 and 5 wt.% TiO_2, and sintering of the product powder, which is

473 comparable to the perovskite phase fraction in similar zirconolite compositions

474 produced by reactive sintering in air [47].

475 **5. CONCLUSION**

476 Molten salt mediated synthesis of zirconolite ceramics, in the context of the

477 decontamination of pyroprocessing molten salt wastes to yield a zirconolite

478 ceramic, has some potential. However, this approach would not offer any clear

479 benefit over oxygen sparging of the salt to precipitate lanthanides and minor

480 actinides as oxides, followed by recovery and immobilisation in a glass or

481 ceramic matrix, since both processes would require subsequent high

482 temperature melting or reactive sintering steps to produce a wasteform

483 monolith. Likewise, in the context of plutonium stockpile immobilisation,

484 although molten salt mediated synthesis of zirconolite reduces the required

485 reaction time and temperature, the subsequent requirement for a consolidation

486 step means that the molten salt method does not offer a compelling advantage.

487 Nevertheless, this work has served to usefully clarify mechanistic aspects of the

488 molten salt mediated synthesis of zirconolite which should inform future

489 application of molten salt technology in the nuclear and wider fields.

490

506 **References**

507 [1] T. Nishimura, T. Koyama, M. Iizuka, H. Tanaka, Development of an environmentally

508   benign reprocessing technology - pyrometallurgical reprocessing technology, Prog. Nucl.

509   Energy. 32 (1998) 381–387. doi:10.1016/S0149-1970(97)00032-2.

510 [2] National Nuclear Laboratory, Advanced Reprocessing Research and Development

511   Needs: Position Paper, Natl. Nucl. Lab. (2015).

512   http://www.nnl.co.uk/media/1672/advanced-reprocessing-position-paper-final.pdf.

513 [3] I.W. Donald, Waste Immobilisation in Glass and Ceramic Based Hosts, Wiley,

514   Chichester, 2010.

24

515   [4]   A.R. Mason, S.M. Thornber, M.C. Stennett, L.J. Gardner, D. Lützenkirchen-Hecht, N.C.

516   Hyatt, Preliminary investigation of chlorine speciation in zirconolite glass-ceramics for

517   plutonium residues by analysis of Cl K-edge XANES, MRS Adv. (2019) 1–7.

518   doi:10.1557/adv.2019.460.

519   [5]   K.A. Evans, J.A. Mavrogenes, H.S. O'Neill, N.S. Keller, L.-Y.Y. Jang, A preliminary

520   investigation of chlorine XANES in silicate glasses, Geochemistry, Geophys.

521   Geosystems. 9 (2008). doi:10.1029/2008GC002157.

522   [6]   D.A. McKeown, H. Gan, I.L. Pegg, W.C. Stolte, I.N. Demchenko, X-ray absorption

523   studies of chlorine valence and local environments in borosilicate waste glasses, J. Nucl.

524   Mater. 408 (2011) 236–245. doi:10.1016/j.jnucmat.2010.11.035.

525   [7]   J.D. Webster, The exsolution of magmatic hydrosaline chloride liquids, Chem. Geol. 210

526   (2004) 33–48. doi:10.1016/j.chemgeo.2004.06.003.

527   [8]   B.D. Begg, E.R. Vance, The incorporation of cerium in zirconolite, Mat. Res. Soc. Symp.

528   Proc. 465 (1997) 333–340. doi:10.1557/PROC-465-333.

529   [9]   M.R. Gilbert, C. Selfslag, M. Walter, M.C. Stennett, J. Somers, N.C. Hyatt, F.R. Livens,

530   Synthesis and characterisation of Pu-doped zirconolites - $(Ca_{1-x}Pu_x)Zr(Ti_{2-2x}Fe_{2x})O_7$, IOP

531   Conf. Ser. Mater. Sci. Eng. 9 (2010). doi:10.1088/1757-899X/9/1/012007.

532   [10]   T.J. White, R.L.L. Segall, J.L.L. Hutchison, J.C.C. Barry, Polytypic behaviour of

533   zirconolite, Proc. R. Soc. Lond. A. 392 (1984) 343–358. doi:10.1098/rspa.1984.0035.

534   [11]   E.R. Vance, B.D. Begg, R.A. Day, C.J. Ball, Zirconolite rich ceramics for actinide wastes,

535   Mat. Res. Soc. Symp. Proc. 353 (1995) 767–774.

536   [12]   D. Caurant, P. Loiseau, I. Bardez, A. Quintas, Glasses, Glass-ceramics and Ceramics

537   for Immobilization of Highly Radioactive Nuclear Wastes, Nova Science Publishers,

538   2009.

539   [13]   G.R. Lumpkin, R.C. Ewing, B.C. Chakoumakos, R.B. Greegor, F.W. Lytle, E.M. Foltyn,

540   F.W. Clinard, L.A. Boatner, M.M. Abraham, Alpha-recoil damage in zirconolite

541   (CaZrTi$_2$O$_7$), J. Mater. Res. 1 (1986) 564–576. doi:10.1557/JMR.1986.0564.

542   [14]   G.R. Lumpkin, R.C. Ewing, Geochemical alteration of pyrochlore group minerals:

543   Betafite subgroup, Am. Mineral. 81 (1996) 1237–1248. doi:10.2138/am-1996-9-1022.

544   [15]   G.R. Lumpkin, K.P. Hart, P.J. McGlinn, T.E. Payne, R. Gieré, C.T. Williams, Retention of

545   actinides in natural pyrochlores and zirconolites, Radiochim. Acta. 66/67 (1994) 469–

546   474. doi:10.1524/ract.1994.6667.s1.469.

547   [16]   R. Gieré, C.T. Williams, G. Lumpkin, Chemical characteristics of natural zirconolite,

548   Swiss Soc. Mineral. Petrol. 78 (1998) 433–459. doi:10.5169/seals-59299.

549   [17]   M.L. Hand, M.C. Stennett, N.C. Hyatt, Rapid low temperature synthesis of a titanate

550   pyrochlore by molten salt mediated reaction, J. Eur. Ceram. Soc. 32 (2012) 3211–3219.

551   doi:10.1016/j.jeurceramsoc.2012.04.046.

552   [18]   T. Advocat, F. Jorion, T. Marcillat, G. Leturcq, X. Deschanels, J.M. Boubals, L. Bojat, P.

553   Nivet, S. Peuget, Fabrication of Pu-Zirconolite Ceramic Pellets by Natural Sintering, Mat.

554   Res. Soc. Symp. Proc. 807 (2004) 1–5. doi:10.1557/PROC-807-267.

555   [19]   M.R. Gilbert, Molten salt synthesis of zirconolite polytypes, Mat. Res. Soc. Symp. Proc.

556   1665 (2014) 325–330. doi:10.1557/opl.2014.662.

557   [20]   T. Kimura, Molten Salt Synthesis of Ceramic Powders, in: C. Sikalidis (Ed.), Adv. Ceram.

558   - Synth. Charact. Process. Specif. Appl., InTech Open, 2011: pp. 75–100.

559   doi:10.5772/20472.

560   [21]   Z. Li, W.E. Lee, S. Zhang, Low-Temperature Synthesis of CaZrO$_3$ Powder from Molten

561   Salts, J. Am. Ceram. Soc. 90 (2007) 364–368. doi:10.1111/j.1551-2916.2006.01383.x.

562   [22]   S. Zhang, Low Temperature Synthesis of Complex Refractory Oxide Powders From

563   Molten Salts, J. Pakistan Mater. Soc. 1 (2007) 49–53.

564   [23]   S. Zhang, D.D. Jayaseelan, G. Bhattacharya, W.E. Lee, Molten salt synthesis of

565   magnesium aluminate (MgAl$_2$O$_4$) spinel powder, J. Am. Ceram. Soc. 89 (2006) 1724–

566   1726. doi:10.1111/j.1551-2916.2006.00932.x.

567   [24]   S. Hashimoto, S. Zhang, W.E. Lee, A. Yamaguchi, Synthesis of Magnesium Aluminate

568   Spinel Platelets from α-Alumina Platelet and Magnesium Sulfate Precursors, J. Am.

569   Ceram. Soc. 86 (2003) 1959–1961. doi:10.1111/j.1151-2916.2003.tb03589.x.

570   [25]   X. Liu, S. Zhang, Low-temperature preparation of titanium carbide coatings on graphite

571   flakes from molten salts, J. Am. Ceram. Soc. 91 (2008) 667–670. doi:10.1111/j.1551-

572   2916.2007.02184.x.

573   [26]   S.M. Thornber, P.G. Heath, G.P. Da, M.C. Stennett, N.C. Hyatt, The effect of pre-

574   treatment parameters on the quality of glass-ceramic wasteforms for plutonium

575   immobilisation, consolidated by hot isostatic pressing, J. Nucl. Mater. 485 (2017).

576   doi:10.1016/j.jnucmat.2016.12.028.

577   [27]   N.C. Hyatt, Plutonium management policy in the United Kingdom: The need for a dual

578   track strategy, Energy Policy. 99 (2016). doi:10.1016/j.enpol.2016.08.033.

579   [28]   K. Webb, R. Taylor, C. Campbell, M. Carrott, C. Gregson, J. Hobbs, F. Livens, C. Maher,

580   R. Orr, H. Sims, H. Steele, S. Sutherland-Harper, Thermal Processing of Chloride-

581   Contaminated Plutonium Dioxide, ACS Omega. 4 (2019) 12524–12536.

582   doi:10.1021/acsomega.9b00719.

583   [29]   S. Sutherland-Harper, F. Livens, C. Pearce, J. Hobbs, R. Orr, R. Taylor, K. Webb, N.

584   Kaltsoyannis, Interactions of HCl and H_2O with the surface of PuO_2, J. Nucl. Mater. 518

585   (2019) 256–264. doi:10.1016/j.jnucmat.2019.02.036.

586   [30]   M.R. Gilbert, J.H. Harding, Energetics of Ce and Pu incorporation into zirconolite waste-

587   forms., Phys. Chem. Chem. Phys. 13 (2011) 13021–13025. doi:10.1039/c0cp01478h.

588   [31]   C. Lopez, X. Deschanels, J.M. Bart, J.M. Boubals, C. Den Auwer, E. Simoni, Solubility of

589   actinide surrogates in nuclear glasses, J. Nucl. Mater. 312 (2003) 76–80.

590   doi:10.1016/S0022-3115(02)01549-0.

591   [32]   P.A. Bingham, R.J. Hand, M.C. Stennett, N.C. Hyatt, M.T. Harrison, The Use of

592   Surrogates in Waste Immobilization Studies: A Case Study of Plutonium, Mater. Res.

593   Soc. Symp. Proc. 1107 (2008). doi:10.1557/PROC-1107-421.

594   [33]   National Reserch Council, Electrometallurgical Techniques for DOE Spent Fuel

595   Treatment, National Academy Press, Washington DC, 2000. doi:10.17226/9883.

596   [34]   Department of Energy and Climate Change, Management of the UK's Plutonium Stocks:

597   A consultation response on the proposed justification process for the reuse of plutonium,

598   2013.

599   [35]   OECD Nuclear Energy Agency, Pyrochemical Separations in Nuclear Applications, A

600   Status Report, 2004. http://www.oecd.org/.

601   [36]   A.A. Coelho, J. Evans, I. Evans, A. Kern, S. Parsons, The TOPAS symbolic computation

602   system, Powder Diffr. 26 (2011) 22–25. doi:10.1154/1.3661087.

603   [37]   J.C. Woicik, B. Ravel, D.A. Fischer, W.J. Newburgh, Performance of a four-element Si

604   drift detector for X-ray absorption fine-structure spectroscopy: Resolution, maximum

605   count rate, and dead-time correction with incorporation into the ATHENA data analysis

606   software, J. Synchrotron Radiat. 17 (2010) 409–413. doi:10.1107/S0909049510009064.

607   [38]   J.A. Bearden, A.F. Burr, Reevaluation of X-ray atomic energy levels, Rev. Mod. Phys. 39

608   (1967) 125–142. doi:10.1103/RevModPhys.39.125.

609   [39]   B. Ravel, M. Newville, ATHENA, ARTEMIS, HEPHAESTUS: Data analysis for X-ray

610   absorption spectroscopy using IFEFFIT, J. Synchrotron Radiat. 12 (2005) 537–541.

611   doi:10.1107/S0909049505012719.

612   [40]   B.D. Begg, E.R. Vance, G.R. Lumpkin, Charge Compensation and the Incorporation of

613   Cerium in Zirconolite and Perovskite, Mat. Res. Soc. Symp. Proc. 506 (1998) 79–86.

614   doi:10.1557/proc-506-79.

615   [41]   Y.Z. Cho, G.H. Park, H.C. Yang, D.S. Han, H.S. Lee, I.T. Kim, Minimization of eutectic

616   salt waste from pyroprocessing by oxidative precipitation of lanthanides, J. Nucl. Sci.

617   Technol. 46 (2009) 1004–1011. doi:10.1080/18811248.2009.9711610.

618   [42]   D.P. Reid, M.C. Stennett, N.C. Hyatt, The fluorite related modulated structures of the

619   Gd$_2$(Zr$_{2-x}$Ce$_x$)O$_7$ solid solution: An analogue for Pu disposition, J. Solid State Chem. 191

620   (2012) 2–9. doi:10.1016/j.jssc.2011.12.039.

621   [43]   M.C. Stennett, C.L. Freeman, A.S. Gandy, N.C. Hyatt, Crystal structure and non-

622   stoichiometry of cerium brannerite: Ce$_{0.975}$Ti$_2$O$_{5.95}$, J. Solid State Chem. 192 (2012) 172–

623   178. doi:10.1016/j.jssc.2012.03.057.

624   [44]   A. V. Soldatov, T.S. Ivanchenko, S. Della Longa, A. Kotani, Y. Iwamoto, A. Bianconi,

625   Crystal-structure effects in the Ce L$_3$-edge X-ray-absorption spectrum of CeO$_2$: Multiple-

626   scattering resonances and many-body final states, Phys. Rev. B. 50 (1994) 5074–5080.

627   doi:10.1103/PhysRevB.50.5074.

628   [45]   A. Bianconi, A. Marcelli, H. Dexpert, R. Karnatak, A. Kotani, T. Jo, J. Petiau, Specific

629   intermediate-valence state of insulating 4f compounds detected by L$_3$ X-ray absorption,

630   Phys. Rev. B. 35 (1987) 806–812. doi:10.1103/PhysRevB.35.806.

631   [46]   C.L. Corkhill, D.J. Bailey, F.Y. Tocino, M.C. Stennett, J.A. Miller, J.L. Provis, K.P. Travis,

632   N.C. Hyatt, Role of Microstructure and Surface Defects on the Dissolution Kinetics of

633   CeO$_2$, a UO$_2$ Fuel Analogue, ACS Appl. Mater. Interfaces. 8 (2016) 10562–10571.

634   doi:10.1021/acsami.5b11323.

635   [47]   L.R. Blackburn, S. Sun, L.J. Gardner, E.R. Maddrell, C. Martin, N.C. Hyatt, A systematic

636   investigation of the phase assemblage and microstructure of the zirconolite CaZr$_{1-}$

637       $_x$Ce$_x$Ti$_2$O$_7$ system, J. Nucl. Mater. (2020). doi:10.1016/j.jnucmat.2020.152137.

638   [48]   Y.P. Lan, H.Y. Sohn, A. Murali, J. Li, C. Chen, The formation and growth of CeOCl

639   crystals in a molten KCl-LiCl flux, Appl. Phys. A Mater. Sci. Process. 124 (2018) 1–6.

640   doi:10.1007/s00339-018-2122-3.

641   [49]   B.D. Begg, R.A. Day, A. Brownscombe, Structural effect of Pu substitutions on the Zr-

642   site in zirconolite, Mat. Res. Soc. Symp. Proc. 663 (2001). doi:10.1557/PROC-663-259.

643   [50]   N. V. Zubkova, N. V. Chukanov, I. V. Pekov, B. Ternes, W. Schüller, D.A. Ksenofontov,

644   D.Y. Pushcharovsky, The crystal structure of nonmetamict Nb-rich zirconolite-3T from

645   the Eifel paleovolcanic region, Germany, Zeitschrift Fur Krist. - Cryst. Mater. 233 (2018)

646   463–468. doi:10.1515/zkri-2017-2133.

647   [51] K.L. Smith, G.R. Lumpkin, M.G. Blackford, R.A. Day, K.P. Hart, The durability of synroc,

648   J. Nucl. Mater. 190 (1992) 287–294. doi:10.1016/0022-3115(92)90092-Y.

649   [52] N.C. Hyatt, C.L. Corkhill, M.C. Stennett, R.J. Hand, L.J. Gardner, C.L. Thorpe, The

650   HADES Facility for High Activity Decommissioning Engineering & Science : part of the

651   UK National Nuclear User Facility, IOP Conf. Ser. Mater. Sci. Eng. 818 (2020) 1–8.

652   doi:10.1088/1757-899X/818/1/012022.

653

654

Figure Captions

Fig. 1. XRD patterns of $Ca_{0.9}Zr_{0.9}Ce_{0.2}Ti_2O_7$ MSS with synthesis temperature: (i)

1400 °C (ii) 1300 °C (iii) 1200 °C (iv) 1100 °C; the reaction time was 2h in air.

Miller indices highlight major reflections of the zirconolite 2M phase. Primary

diagnostic reflections of reagents and accessory phases are indicated by: P,

$CaTiO_3$ perovskite; T, TiO_2 rutile; Z, ZrO_2; C, CeO_2.

Fig. 2. Quantitative phase analysis of XRD data of MSS products shown in

Fig. 1 and Fig. 3-5; "excess" denotes addition of 10 wt.% ZrO_2 and 5 wt.% TiO_2

to stoichiometric formulation. Unless otherwise stated MSS was performed at

1200 °C for 2 h in air with CeO_2 as the Ce source.

Fig. 3. XRD patterns of $Ca_{0.9}Zr_{0.9}Ce_{0.2}Ti_2O_7$ MSS at 1200 °C for 2 h, with

synthesis atmospheres: (i) air (ii) 5% H_2/N_2 (iii) Ar. Miller indices highlight major

reflections of the zirconolite 2M phase. Primary diagnostic reflections of

reagents and accessory phases are indicated by: P, $CaTiO_3$ perovskite; T, TiO_2;

Z, ZrO_2; C, CeO_2.

Fig. 4. XRD patterns of $Ca_{0.9}Zr_{0.9}Ce_{0.2}Ti_2O_7$ MSS at 1200 °C in air with furnace

dwell durations: (i) 8 h (ii) 4 h (iii) 2 h. Miller indices highlight major reflections of

the zirconolite 2M phase. Primary diagnostic reflections of reagents and

accessory phases are indicated by: P, $CaTiO_3$ perovskite; T, TiO_2; Z, ZrO_2; C,

CeO_2.

Fig. 5. XRD patterns of $Ca_{0.9}Zr_{0.9}Ce_{0.2}Ti_2O_7$ MSS with additional excesses of 10

wt.% ZrO_2 and 5 wt.% TiO_2, and $CeCl_3$ reagent where indicated: (i) 1200 °C,

$CeCl_3$, 10 wt.% ZrO_2 and 5 wt.% TiO_2 (ii) 1200 °C, $CeCl_3$ (iii) 1200 °C,10 wt.%

678   ZrO_2 and 5 wt.% TiO_2 (iv) 1200 °C; the reaction time was 2 h, in air. Miller

679   indices highlight major reflections of the zirconolite 2M phase. Primary

680   diagnostic reflections of reagents and accessory phases are indicated by: P,

681   $CaTiO_3$ perovskite; T, TiO_2; Z, ZrO_2; C, CeO_2.

682   Fig. 6. XRD patterns to compare; (i) the product of a secondary sintering

683   process (1350 °C, for 20 h, in air) of the MSS product in (ii), (ii)

684   $Ca_{0.9}Zr_{0.9}Ce_{0.2}Ti_2O_7$ MSS; 1200 °C for 2 h in air. Miller indices highlight major

685   reflections of the zirconolite 2M phase. Primary diagnostic reflections of

686   reagents and accessory phases are indicated by: P, $CaTiO_3$ perovskite; T, TiO_2;

687   Z, ZrO_2; C, CeO_2.

688   Fig. 7. SEM micrographs, in secondary electron mode, of: (A) TiO_2 (B) CeO_2 (C)

689   ZrO_2 (D) $Ca_{0.9}Zr_{0.9}Ce_{0.2}Ti_2O_7$ from MSS at 1200 °C, for 2h, in air.

690   Fig. 8. SEM micrograph, in SE mode, of the surface of the ceramic produced

691   after sintering of MSS product at 1350 °C for 20 h, in air, highlighting

692   component phases: accessory phases are indicated by: P, perovskite; Z, ZrO_2;

693   and zirconolite 2M and 4M polymorphs. Representative EDX spectrum of the

694   zirconolite 2M phase is shown.

695   Fig. 9. Ce L_3 XANES spectra of recovered product of $Ca_{0.9}Zr_{0.9}Ce_{0.2}Ti_2O_7$ MSS

696   in air, compared with $CePO_4$, $CeAlO_3$ and CeO_2 reference compounds: A)

697   reaction at 1100 – 1400 °C for 2 h, in air; B) reaction at 1200 °C for 2 h using

698   flowing 5% H_2/N_2, Ar or air; C) reaction at 1200 °C for 2 – 8 h, in air; D) reaction

699   at 1200 °C for 2 h, in air, using CeO_2 or $CeCl_3.7H_2O$ as Ce source, with / without

700   10 wt.% ZrO_2 and 5 wt.% TiO_2 excess.

701   Fig. 10. Comparison of quantity of Ce^{3+} and perovskite weight fraction in

702   product materials. Black squares represent all MSS zirconolite materials

703   produced at 1200 °C. Blue circles represent MSS zirconolite materials produced

704   at temperatures other than 1100 °C, 1300 °C and 1400 °C.

705 **Tables**

Temperature (°C)	Time (h)	Atmosphere	Reagent	Excess	Phase fraction (wt.%)						
					CaTiO$_3$ (± 1.0)	CeO$_2$ (± 0.07)	TiO$_2$ (± 0.2)	Z-2M (± 1.8)	Z-3T (± 1.5)	Z-4M (± 1.5)	ZrO$_2$ (± 0.4)
1100	2	air	CeO$_2$	-	32.8	0.40	2.1	43.9	11.0	0	9.7
1200	2	air	CeO$_2$	-	28.1	0.16	1.7	52.2	14.7	0	3.0
1300	2	air	CeO$_2$	-	27.3	0.20	2.1	52.4	15.8	0	2.1
1400	2	air	CeO$_2$	-	24.8	0.27	0.2	62.1	12.2	0	0.3
1200	4	air	CeO$_2$	-	27.5	1.11	1.7	56.7	9.8	0	3.9
1200	8	air	CeO$_2$	-	26.6	0.62	0.2	53.8	16.2	0	2.4
1200	2	air	CeO$_2$	✓	9.4	0.26	1.8	64.3	19.3	0	3.9
1200	2	air	CeCl$_3$	-	25.4	0.62	3.0	47.1	15.7	0	8.0
1200	2	air	CeCl$_3$	✓	15.4	0.33	3.7	48.5	20.4	0	11.5
1200	2	5% H$_2$/N$_2$	CeO$_2$	-	33.3	0.58	2.1	30.7	15.9	0	17.2
1200	2	Ar	CeO$_2$	-	40.9	0.28	8.4	29.1	5.7	0	15.6
1350**	20	air	CeO$_2$	-	7.3	0.12	0.1	75.9	5.8	10.0	0.7

706

707 Table 1. Quantitative analysis using Rietveld refinement on XRD patterns in Fig. 1 and Fig. 3-5; "excess" denotes addition of

708 10 wt.% ZrO$_2$ and 5 wt.% TiO$_2$ to stoichiometric formulation. ** Refers to the material produced after the secondary sintering of

709 the MSS material formed at 1200 °C for 2 h in air with CeO$_2$ as the surrogate.

34

Temperature (°C)	Time (h)	Atmosphere	Reagent	Excess	Ce^{3+} (%)
1100	2	Air	CeO_2	-	54 ± 3
1200	2	Air	CeO_2	-	59 ± 3
1300	2	Air	CeO_2	-	62 ± 3
1400	2	Air	CeO_2	-	71 ± 3
1200	4	Air	CeO_2	-	62 ± 3
1200	8	Air	CeO_2	-	53 ± 3
1200	2	Air	CeO_2	✓	33 ± 3
1200	2	Air	$CeCl_3$	-	38 ± 3
1200	2	Air	$CeCl_3$	✓	33 ± 3
1200	2	5% H_2/N_2	CeO_2	-	100 ± 4
1200	2	Ar	CeO_2	-	100 ± 4

710

711   Table 2. Results of linear combination fitting of spectra from Fig. 9.; "excess" denotes addition of 10 wt.% ZrO_2 and 5 wt.%

712   TiO_2 to the stoichiometric formulation.
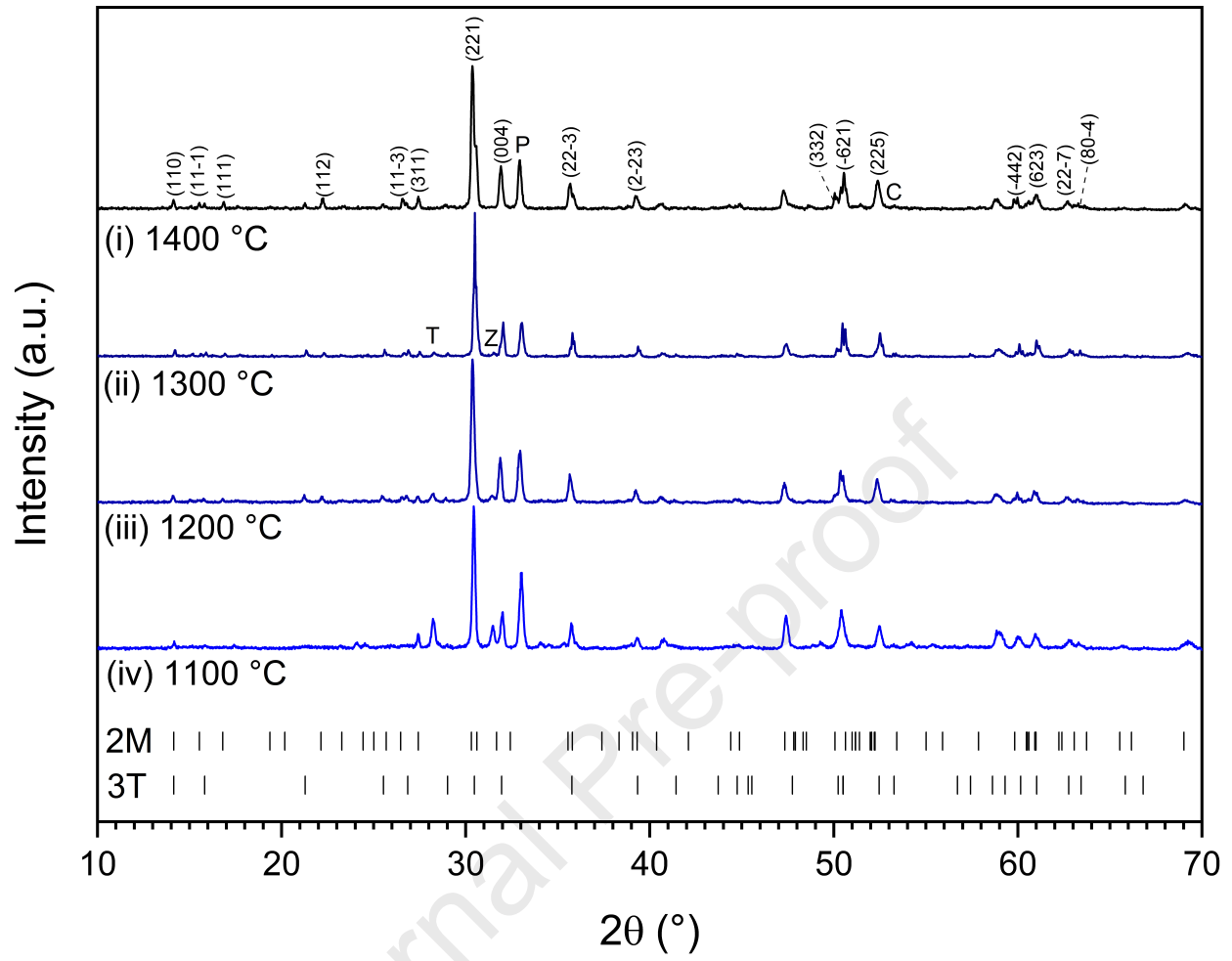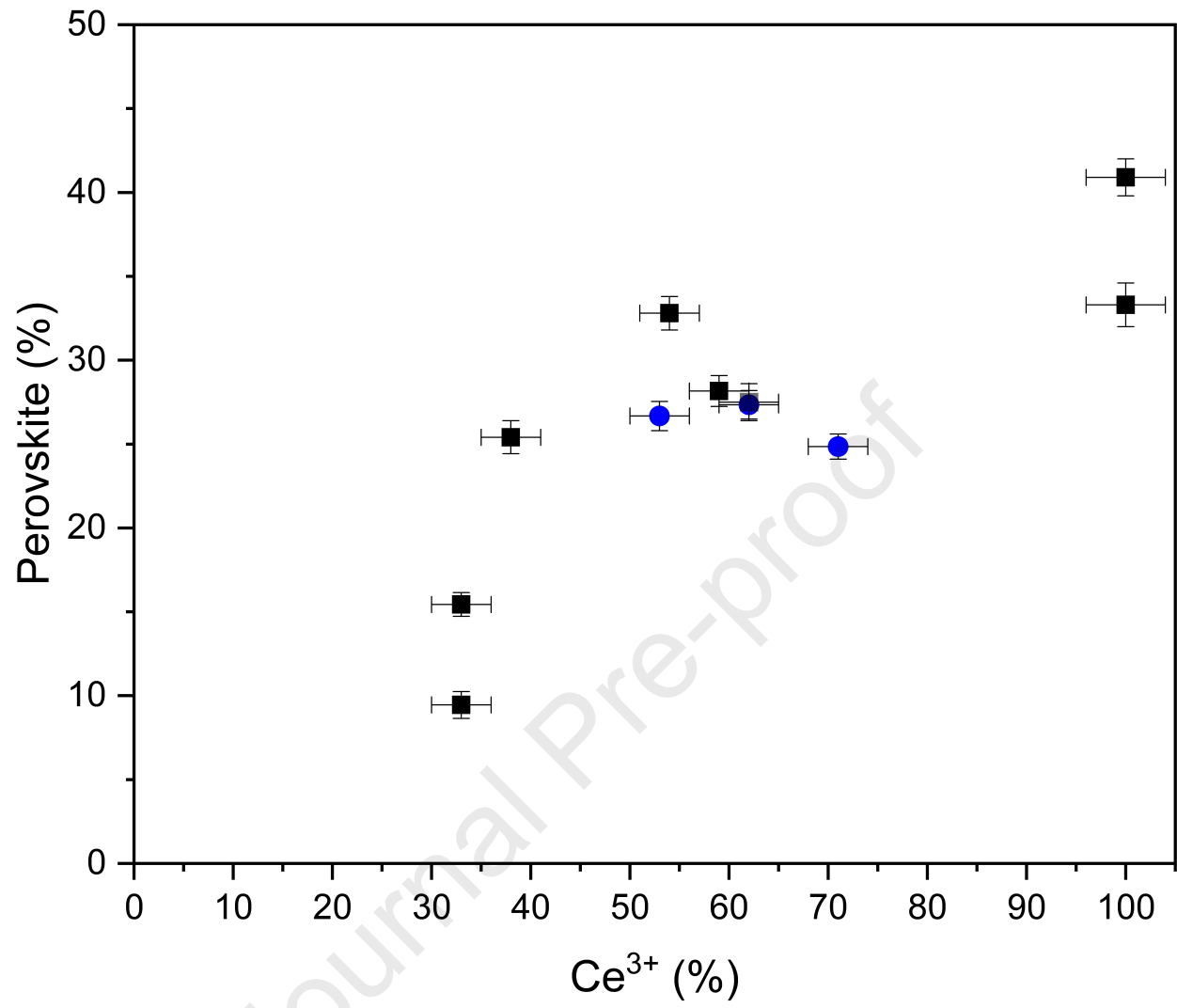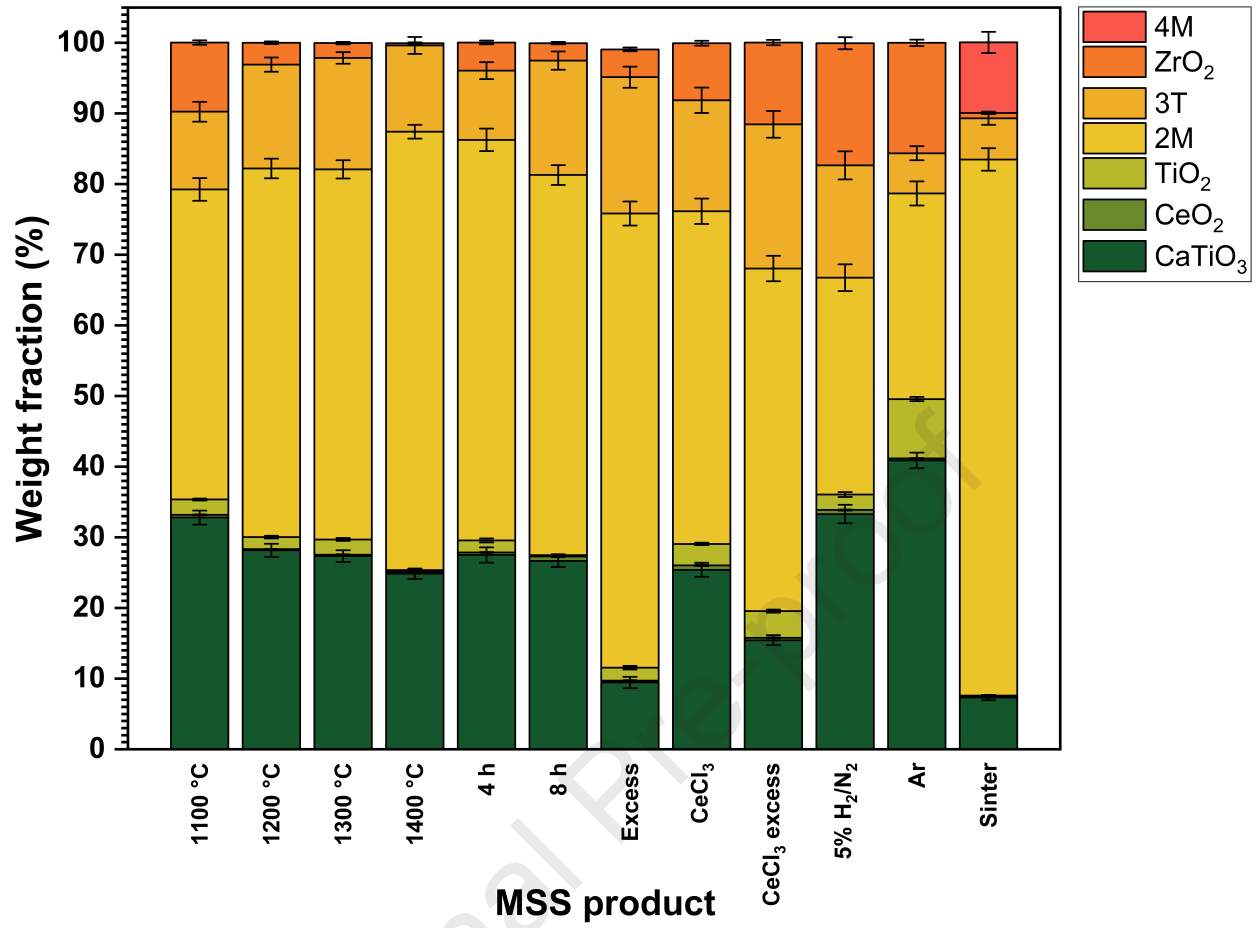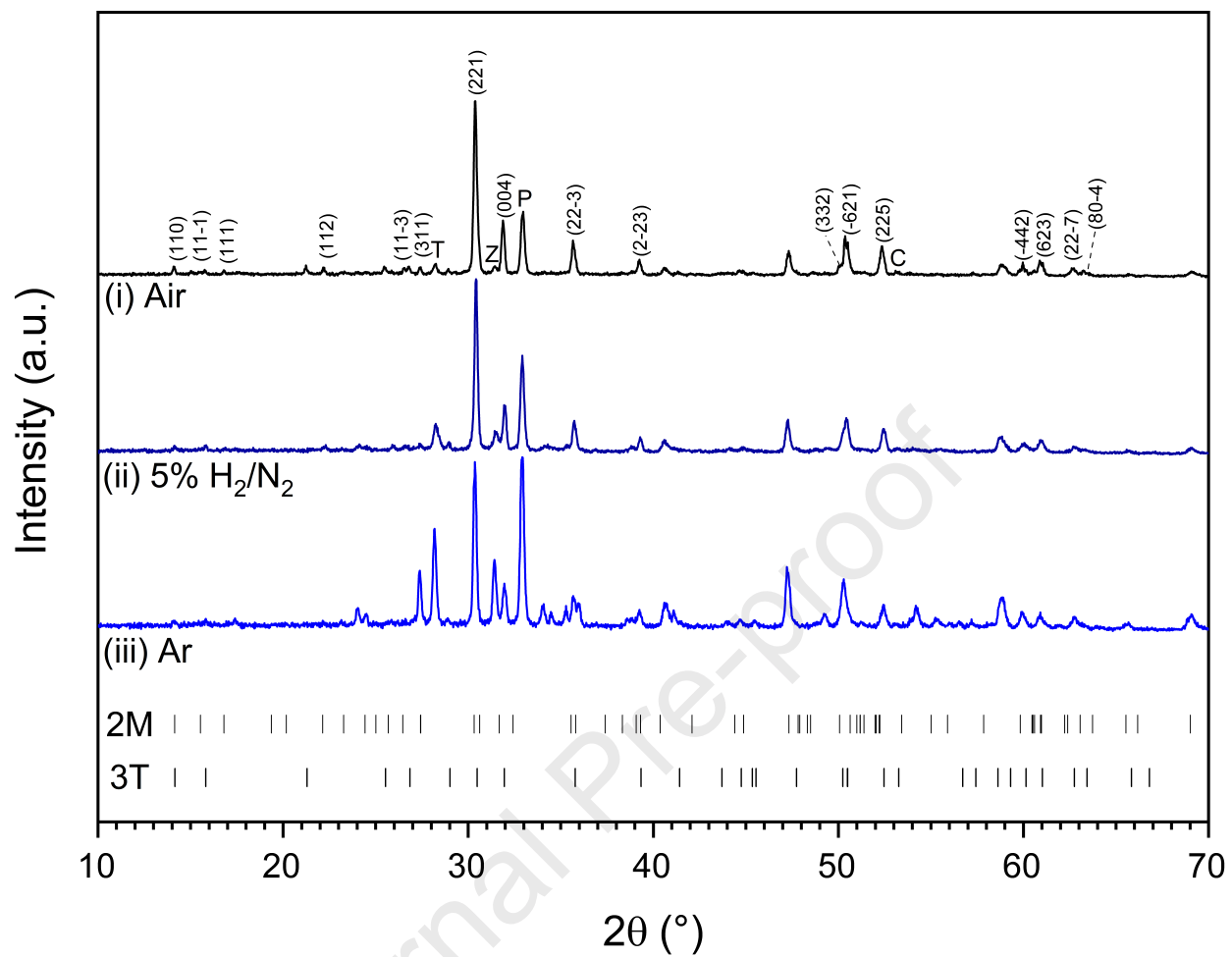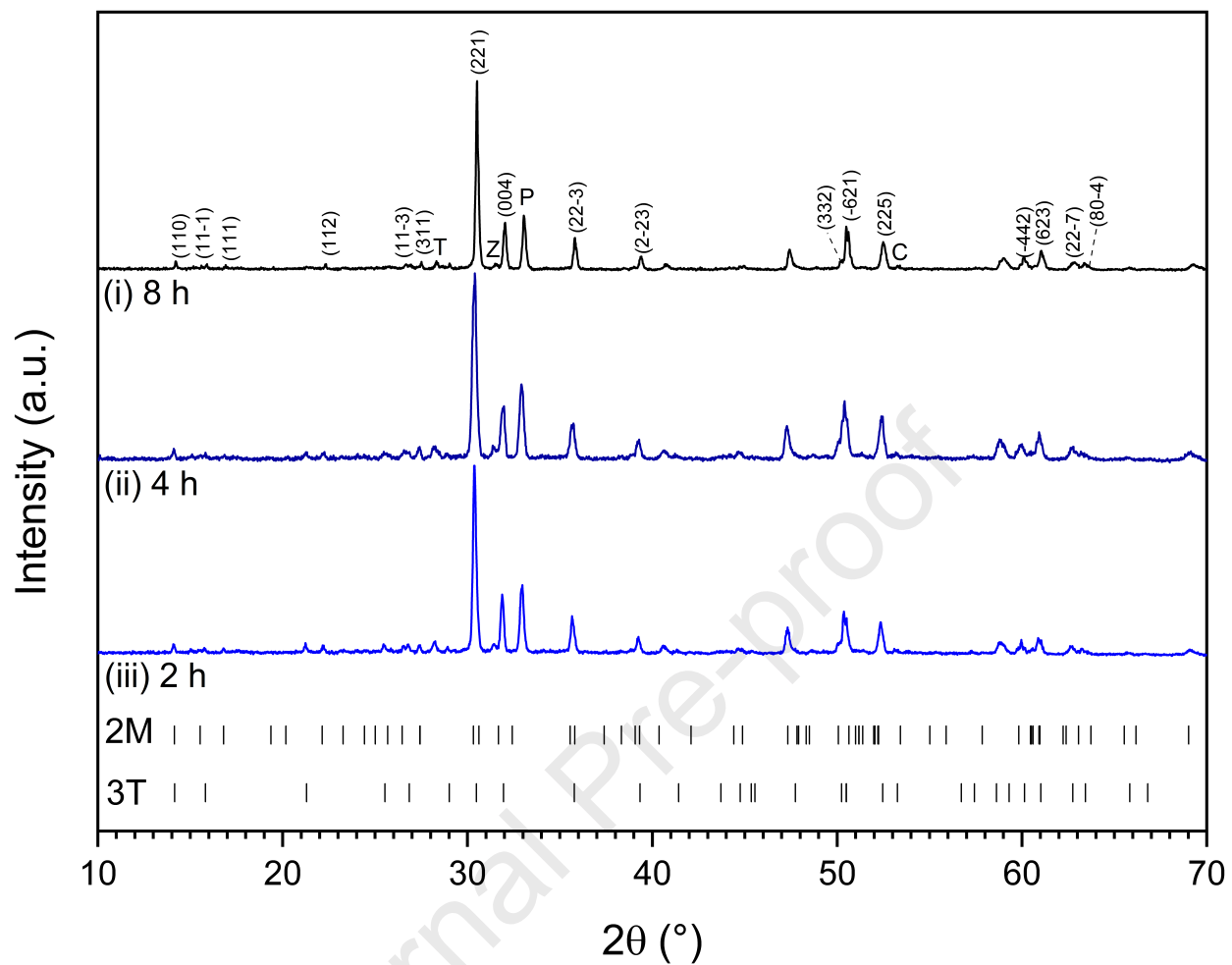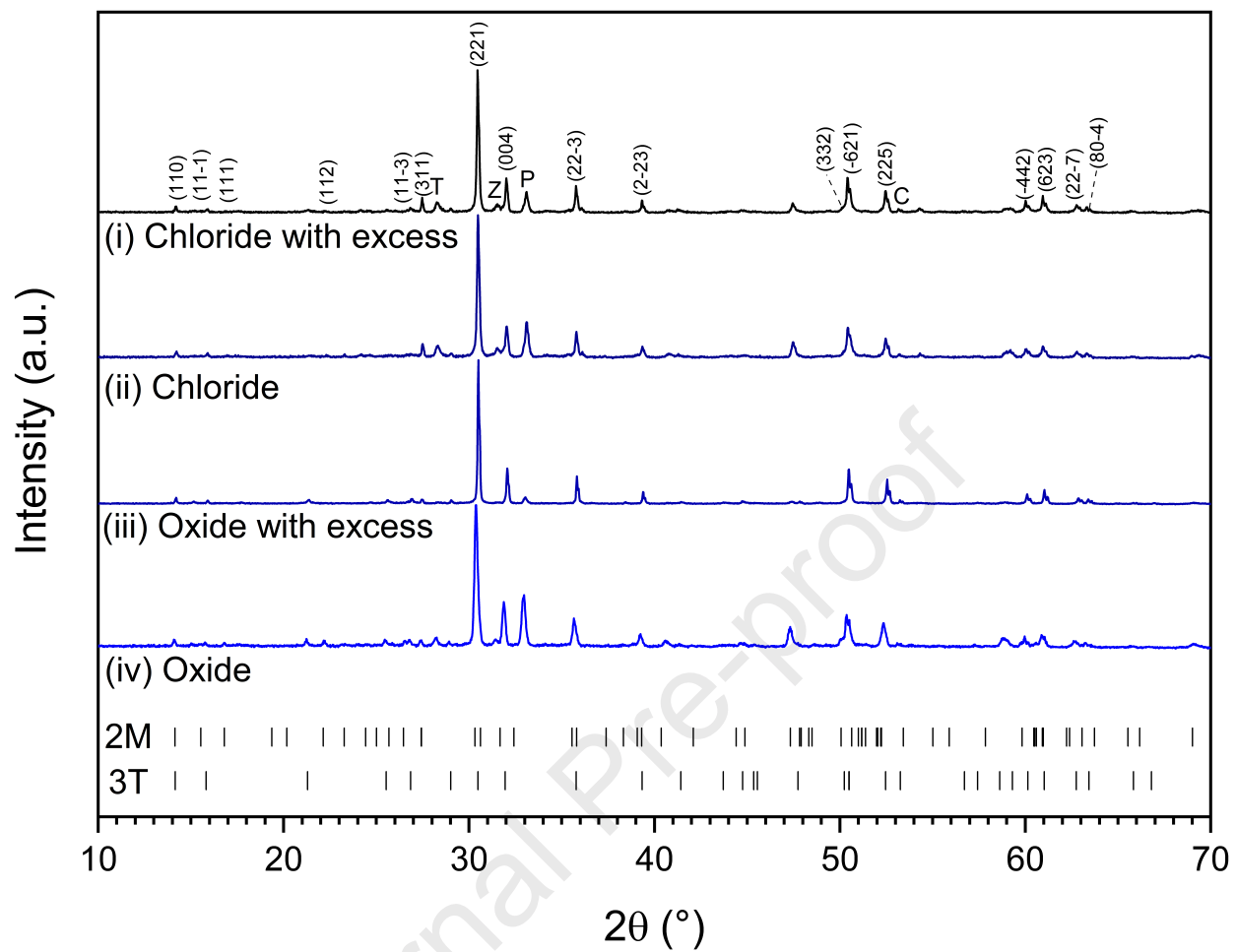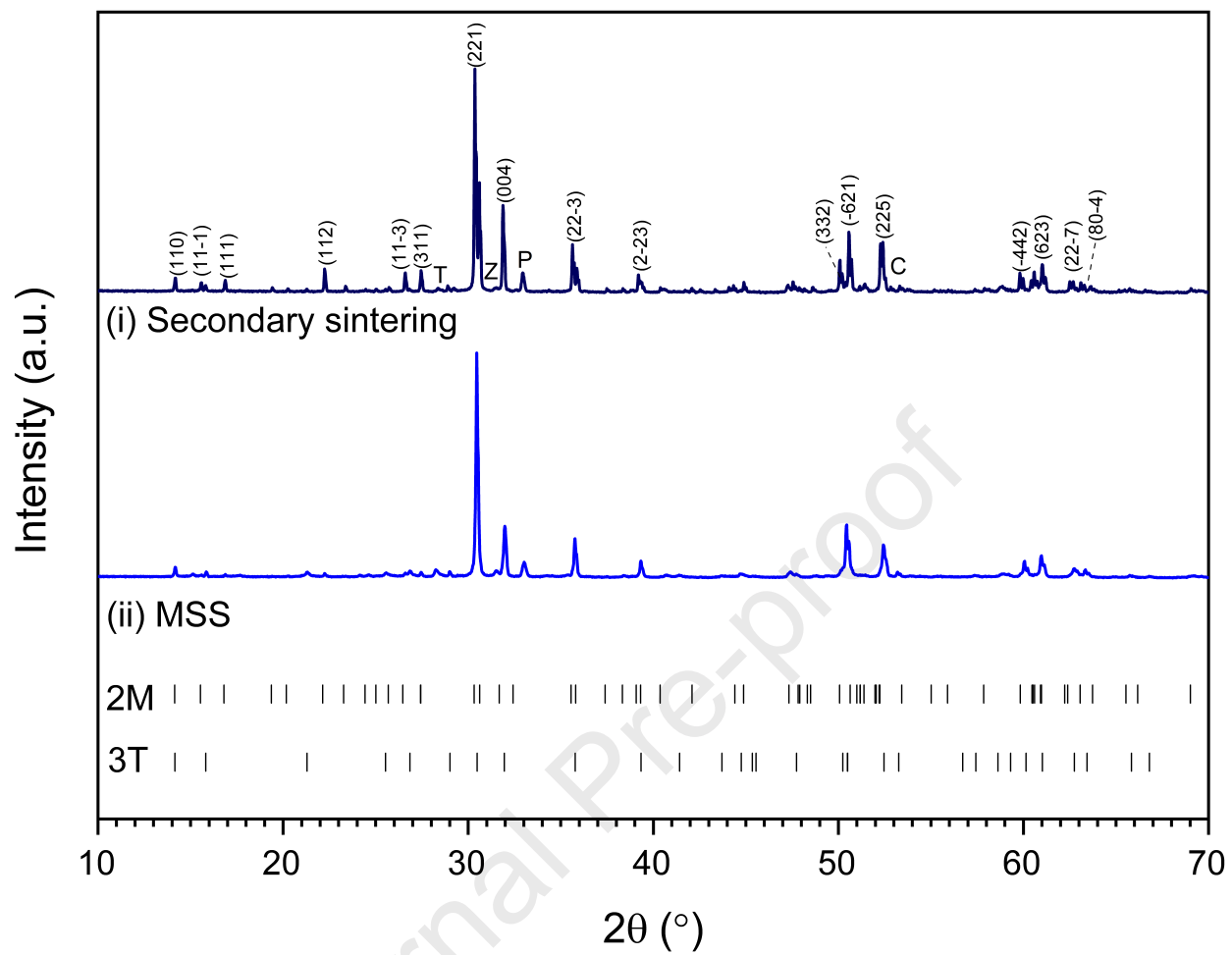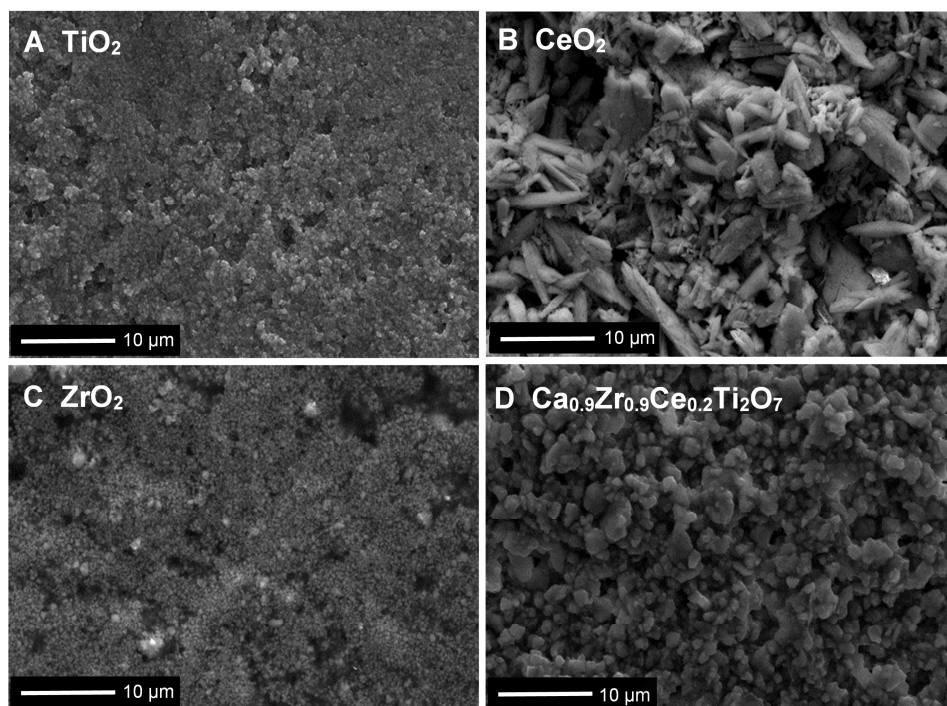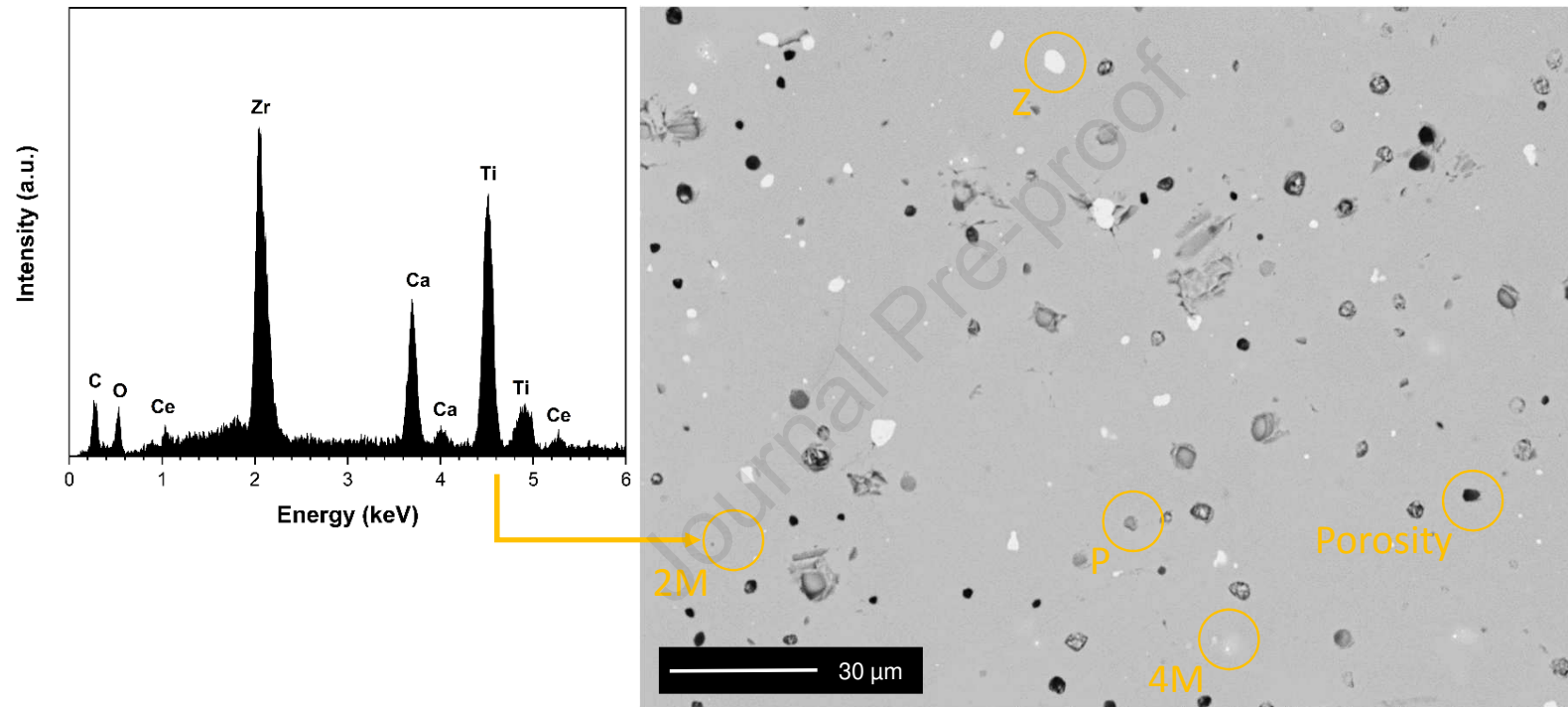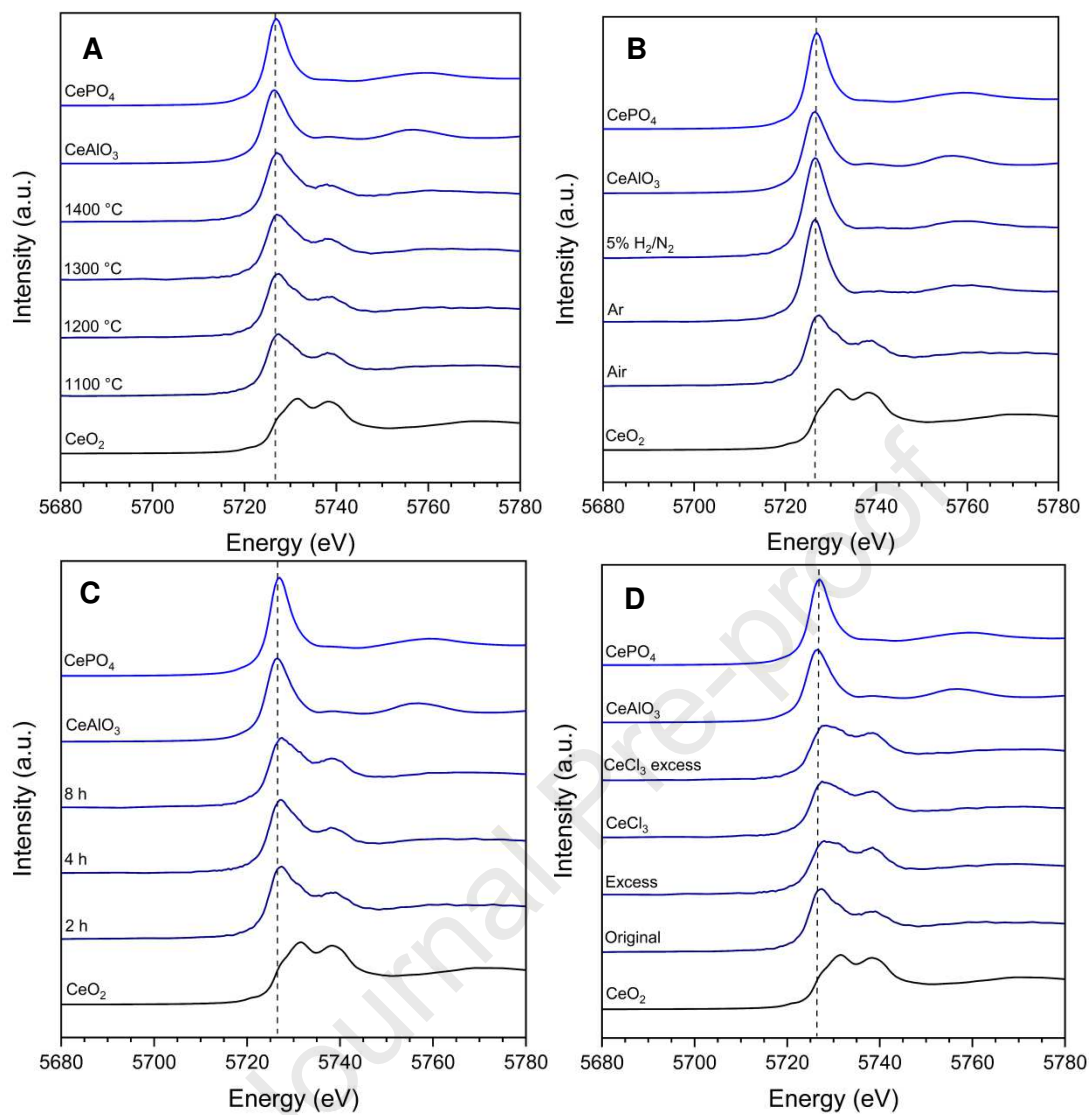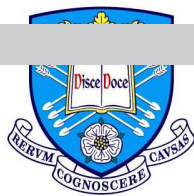
35

713

(i) Secondary sintering

(ii) MSS

2M

3T

Intensity (a.u.)

2θ (°)

Professor Neil Hyatt
Royal Academy of Engineering Chair in Radioactive Waste Management
Professor of Nuclear Materials Chemistry
Sir Robert Hadfield Building
Mappin Street
Sheffield S1 3JD
United Kingdom
Telephone: +44 (0) 114 222 5502
e-mail: n.c.hyatt@sheffield.ac.uk

30 July 2020

Dear Editor,

I am pleased to submit the attached revised manuscript titled *"Molten salt synthesis of Ce doped zirconolite for the immobilisation of pyroprocessing wastes and separated plutonium"* by Mason *et al.*, to be considered for publication in Ceramics International. I confirm that the manuscript is not under consideration for publication elsewhere, that its publication is approved by all authors, and that, if accepted, it will not be published elsewhere in the same form, in English or in any other language, including electronically without the written consent of the copyright-holder.

The manuscript has been amended in response to each comment from the two reviewers, with the requested change being implemented in each case. This is detailed in the attached "Response to Reviewers" documents. We have also made some minor changes to the text and tables to improve clarity, prompted by feedback from the reviewers, including the addition of three supplementary figures for completeness.

On behalf of the co-authors may I take this opportunity to thank the two reviewers for their careful reading of the manuscript and suggestions for improvement, and also the editorial team for their handling of the manuscript at this challenging time.

Thank you for your consideration of our manuscript. Please contact me at the above email address with correspondence.

Yours sincerely

Professor Neil Hyatt.

Declaration of interests

☒ The authors declare that they have no known competing financial interests or personal relationships that could have appeared to influence the work reported in this paper.

☐The authors declare the following financial interests/personal relationships which may be considered as potential competing interests: